Geochemistry, Geophysics, Geosystems®

RESEARCH ARTICLE
10.1029/2023GC010964

Crystallization of Superfast-Spreading Oceanic Crust (ODP Hole 1256D, Pacific Ocean): Constraints From Zircon Geochronology

C. Johan Lissenberg[1], Daniel J. Condon[2], Andrew J. Smye[3], and Ryo Anma[4]

[1]School of Earth and Environmental Sciences, Cardiff University, Cardiff, UK, [2]British Geological Survey, Keyworth, UK, [3]Department of Geosciences, The Pennsylvania State University, University Park, PA, USA, [4]Graduate School of Technology, Industrial and Social Sciences, Tokushima University, Tokushima, Japan

Abstract Studies of oceanic crust, which covers a large proportion of the Earth's surface, have provided significant insight into the dynamics of crustal accretion processes at mid-ocean ridges. It is now recognized that the nature of oceanic crust varies fundamentally as a function of spreading rate. Ocean Drilling Program (ODP) Hole 1256D (eastern Pacific Ocean) was drilled into the crust formed at a superfast spreading rate, and hence represents a crustal end member. Drilling recovered a section through lava and sheeted dykes and into the plutonic sequence, the study of which has yielded abundant insight into magmatic and hydrothermal processes operating at high spreading rates. Here, we present zircon U-Pb dates for Hole 1256D, which constrain the age of the section, as well as the duration of crustal accretion. We find that the main pulse of zircon crystallization within plutonic rocks occurred at 15.19 Ma, consistent with magnetic anomalies, and lasted tens of thousands of years. During this episode, the main plutonic body intruded, and partial melts of the base of the sheeted dykes crystallized. One sample appears to postdate this episode by up to 0.25 Myr, and may be an off-axis intrusion. Overall, the duration of crustal accretion was tens to several hundreds of thousands of years, similar to that found at the fast-spreading East Pacific Rise and the slow-spreading Mid-Atlantic Ridge. This indicates that crustal accretion along slow- to superfast-spreading ridges occurs over similar time scales, with substantially longer periods of accretion occurring at ultraslow-spreading ridges characterized by thick lithosphere.

Plain Language Summary The oceanic crust paves approximately 2/3 of the Earth's surface. It is formed at mid-ocean ridges, where tectonic plates separate and new crust is formed by the solidification of magma. This magma is formed by partial melting of the upper mantle beneath the ridge axis. Plates spread at different rates at different mid-ocean ridges, and the fastest-known spreading occurred some 11–18 million years ago in the eastern Equatorial Pacific. A section of the crust formed during this episode of superfast-spreading was recovered by scientific drilling in the framework of the Integrated Ocean Drilling Program (IODP). This study presents age data that determine when this section of superfast-spreading crust formed, and how long it took to build the crust. We find that the age of the section is 15.19 Ma, and that crustal formation lasted between tens and several hundreds of thousands of years. This duration is similar to that found at mid-ocean ridges with slow- to fast-spreading rates, such as the Mid-Atlantic Ridge and East Pacific Rise. However, it is much shorter than the formation of crust at ultraslow-spreading ridges, where the cool and thick nature of the lithosphere leads to prolonged episodes of crustal formation.

Key Points:

- The main pulse of crystallization of superfast-spreading crust at Hole 1256D occurred at 15.19 Ma
- Crustal accretion lasted between tens and several hundreds of thousands of years
- Crustal accretion along slow- to superfast-spreading ridges occurs over similar time scales

Supporting Information:

Supporting Information may be found in the online version of this article.

Correspondence to:

C. J. Lissenberg,
lissenbergcj@cardiff.ac.uk

Citation:

Lissenberg, C. J., Condon, D. J., Smye, A. J., & Anma, R. (2023). Crystallization of superfast-spreading oceanic crust (ODP Hole 1256D, Pacific Ocean): Constraints from zircon geochronology. *Geochemistry, Geophysics, Geosystems*, *24*, e2023GC010964. https://doi.org/10.1029/2023GC010964

Received 22 MAR 2023
Accepted 22 SEP 2023

Author Contributions:

Conceptualization: C. Johan Lissenberg
Funding acquisition: C. Johan Lissenberg
Investigation: C. Johan Lissenberg, Daniel J. Condon, Andrew J. Smye
Methodology: Daniel J. Condon, Andrew J. Smye
Resources: Ryo Anma
Validation: Daniel J. Condon, Andrew J. Smye
Visualization: C. Johan Lissenberg
Writing – original draft: C. Johan Lissenberg

1. Introduction

Oceanic crust forms continuously along mid-ocean ridges in response to the plate separation, during a hallmark process of plate tectonics. The dynamics of the formation of oceanic crust at mid-ocean ridges has been the subject of debate since their discovery in the 1950s. There is now consensus that there are first-order differences in crustal accretion processes and the resulting lithospheric architecture between fast-, slow-, and ultraslow-spreading mid-ocean ridges (Dick et al., 2003). At fast-spreading ridges, the crust appears to have a fairly uniform thickness of 6–7 km (Chen, 1992; White et al., 1992) and conforms to the classic Penrose-type igneous sequence of lava, sheeted dykes and gabbroic rocks overlying mantle peridotite (Conference Participants, 1972). This is in keeping with observations from geophysical studies, which show a robust magmatic system characterized by a melt-rich body at the top of the lower crust, overlying lower-crustal-scale crystal mush (Carbotte et al., 2013; Crawford & Webb, 2002; Dunn et al., 2000; Marjanović et al., 2018; Sinton & Detrick, 1992). At slower spreading rates,

Writing – review & editing: Daniel J. Condon, Andrew J. Smye, Ryo Anma

where mantle upwelling is slower and less melt is produced, the magmatic system is less extensive, with fewer magma reservoirs detected geophysically (Detrick et al., 1990; Sinton & Detrick, 1992). As a result, the tectonic accommodation of extension is more prominent. This leads to the occurrence of long-lived detachment faults, which can exhume lower crustal and mantle rocks onto the seafloor (Cann et al., 1997; Cannat, 1993; Dick et al., 1981; Escartin et al., 2008; Karson & Dick, 1983; Lagabrielle et al., 1998; MacLeod et al., 2002; Mével et al., 1991; Smith et al., 2006). As a result, the oceanic crust does not have a uniform thickness, and is highly variable along-axis. Locally, the crust may only comprise gabbroic plutons in mantle peridotite (Cannat, 1996; Cannat et al., 1997) or be absent entirely (Cannat et al., 2006; Dick et al., 2003; Michael et al., 2003).

Zircon geochronology provides an important—yet underutilized—tool to study the dynamics of crustal accretion at mid-ocean ridges. Through U-Pb and U-Th dating, zircon can provide the absolute dates of crystallization of igneous units, enabling reconstructions of a number of important variables and processes. The first variable is the spreading rate (C. J. Lissenberg et al., 2009). The spreading rate can be reconstructed where precise zircon U-Pb dates are obtained in a section across-axis. This approach was first applied to the Vema Lithospheric Section (11°N, Mid-Atlantic Ridge), where a linear age progression away from the spreading axis revealed a spreading rate of ∼16 mm/yr, in agreement with magnetic anomaly derived plate motion estimates (C. J. Lissenberg et al., 2009).

The second variable is the time span of accretion of the plutonic section (Baines et al., 2009; Grimes et al., 2008; C. J. Lissenberg et al., 2009; Rioux et al., 2016; Rioux, Lissenberg, et al., 2012; Schwartz et al., 2005). Previous studies have shown that the duration of crustal accretion is preserved on the grain scale, the sample scale, as well as the crustal scale. Grain-scale information on the duration of crustal accretion occurs in the form of inherited cores overgrown by younger rims, which show age differences as much as ∼1.5 Ma at the slow- to ultraslow-spreading Southwest Indian Ridge (Schwartz et al., 2005). On a sample scale, different zircon grains from the same sample do not always define a uniform age population, but instead may record hundreds of thousands of years of zircon growth (C. J. Lissenberg et al., 2009; Rioux, Lissenberg, et al., 2012). On a lower crustal scale, age differences of the order of hundreds of thousands of years have been documented between different intrusive series in the (I) ODP drill core from both Atlantic (Grimes et al., 2008) and Indian (Rioux et al., 2016) oceanic core complexes. Overall, zircon U-Pb data have demonstrated that crustal accretion is more protracted than previously assumed; even at the East Pacific Rise, where the relatively fast spreading rate would be expected to lead to rapid accretion, significant intra-sample age spread in zircon dates was recorded (Rioux, Lissenberg, et al., 2012). To date, no straightforward correlation appears to exist between the duration of magmatism and spreading rate.

The third variable that U-Pb zircon dating can resolve is the dynamics of oceanic detachment faults. These detachment faults are now recognized to play a significant role in accretion along slow- and ultraslow-spreading ridges (Cannat et al., 2006; Escartin et al., 2008; Smith et al., 2006). Zircon U-Pb dates can enable reconstructions of the rates of slip on the detachments (Baines et al., 2008; Grimes et al., 2008). This has shown that slip along the detachment faults may accommodate the majority of plate separation during periods of detachment faulting, leading to significant asymmetric spreading (Baines et al., 2008; Grimes et al., 2008). The dates can also be used to determine the depth of crystallization of gabbroic rocks in the footwall of the detachments (C. J. Lissenberg et al., 2016). Furthermore, when combined with zircon (U-Th)/He dates, zircon U-Pb dates enable the depth and thermal structure of the detachment faults to be reconstructed (Grimes et al., 2011; Schoolmeesters et al., 2012).

Integrating zircon U-Pb or U-Th dates with dates for systems with lower closure temperatures (e.g., zircon (U-Th)/He and $^{40}Ar/^{39}Ar$ of associated phases) has enabled reconstructions of the cooling histories for mid-ocean magmatic systems. This has been applied successfully to both plutonic sections (John et al., 2004; Schwartz et al., 2009) and volcanic rocks (Schmitt et al., 2011).

Finally, U-Pb dating of igneous and hydrothermal zircons have been used to determine the age of both magmatic crystallization and hydrothermal alteration of gabbroic rocks at the Vema Lithospheric Section (Mid-Atlantic Ridge; Rioux et al., 2015) and at Atlantis Bank (Southwest Indian Ridge; Schwartz et al., 2010), providing absolute time constraints on alternating cycles of magmatism and hydrothermal fluid flow at mid-ocean ridges.

Combined, studies using zircon geochronology of the oceanic crust have thus led to considerable new insights into the dynamics of oceanic crustal accretion. Here, we present zircon U-Pb dates of plutonic rocks from superfast-spreading crust recovered in Ocean Drilling Program (ODP) Hole 1256D (eastern Pacific Ocean), with the aim of determining its absolute age as well as the time span and dynamics of its accretion. We show that crustal

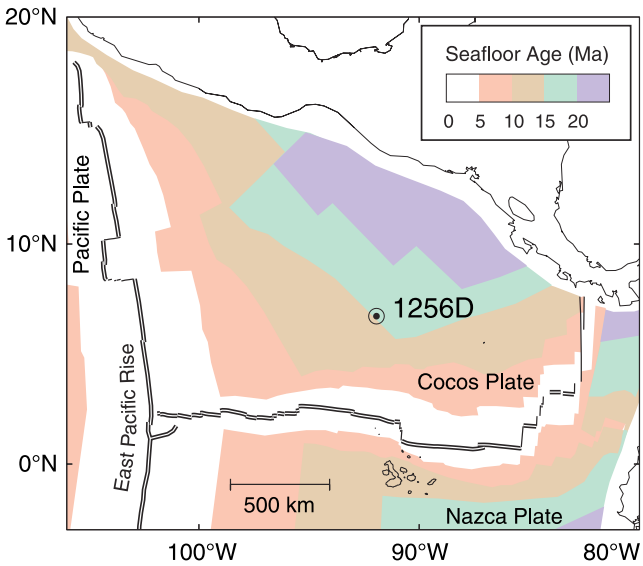

Figure 1. Map showing the location of Ocean Drilling Program Hole 1256D in the eastern Pacific Ocean, along with the seafloor age estimated from magnetic anomaly data (Wilson, 1996). Adapted from Wilson et al. (2006).

accretion was largely completed by 15.19 Ma, but that magmatism may have continued for up to 0.25 Myr. Combined with data from across the spreading rate spectrum, this indicates that the duration of crustal accretion appears to be similar at all spreading rates, with the exception of ultraslow-spreading rates, where accretion may take significantly longer.

2. ODP Hole 1256D

Hole 1256D was drilled in oceanic crust formed during superfast spreading along the Pacific-Cocos plate boundary in the eastern Pacific (Figure 1). This superfast-spreading episode occurred in the middle Miocene (~18–11 Ma), with magnetic anomalies indicating spreading rates as high as 220 mm/yr (Wilson, 1996; Wilson et al., 2006). This is the fastest spreading rate on record; hence, the crust formed during this interval represents an end member configuration of oceanic crust. A section of this crust was drilled over four expeditions of the (Integrated) Ocean Drilling Program ((I)ODP): Expeditions 206, 309, 312, and 335 (Teagle et al., 2006, 2012; Wilson, Teagle, et al., 2003). The underlying rationale relied on the observation that the depth to the lower crustal magmatic system correlates inversely with the spreading rate (Carbotte et al., 1998; Phipps Morgan & Chen, 1993; Purdy et al., 1992); hence, superfast-spreading crust should have a thin upper crust, enabling drilling through a full upper crustal section and into in situ lower oceanic crust (Wilson et al., 2006).

The uppermost basement rocks recovered from Hole 1256D comprise a 284 m thick off-axis lava sequence of sheet flows and pillows, which overlies the axial volcanic sequence (470 m thick) of predominantly sheet and massive flows. These volcanic rocks have typical N-MORB compositions (Cooper, 2007; Neo et al., 2009; Yamazaki et al., 2009). Below a ~50 m thick transition zone, a sheeted dyke complex with a thickness of 346 m was recovered. The thin nature of the sheeted dykes relative to the lava has been attributed to the fact that there appears to be no level of neutral buoyancy in the crust, as well as the relatively high magmatic pressures expected at magma-rich spreading centers, both of which favor extrusion over intrusion (Umino et al., 2008). However, the dykes, on average, are more evolved—and hence denser—than the lavas, suggesting that not all dykes erupted (Sano et al., 2011). This is consistent with their predominantly horizontal flow fabrics, as recorded by magnetic fabrics (Veloso et al., 2014). The lower 115 m of the hole comprised the transition from the upper crust (sheeted dykes and lavas) to the lower crust (plutonic rocks): at 1156 m below the top of the basement, the first gabbroic rocks were recovered (Figure 2). These form a heterogeneous gabbroic body of 54 m thick (referred to as Gabbro 1), which is comprised predominantly of medium-grained rocks that range in composition from modally layered olivine gabbros to oxide gabbros (Teagle et al., 2006, 2012). Gabbros are internally heterogeneous down to the thin section scale, with early, relatively primitive subophitic domains forming patches in a matrix with granular textures and evolved compositions (Koepke et al., 2011). Gabbro 1 is intruded near its top by a thin (<1 m) quartz-rich oxide diorite (Teagle et al., 2006). Following a dyke screen of 54 m thick, a second gabbroic body (Gabbro 2) was recovered, which appears to be a single intrusion of variably oxide-bearing gabbronorite (Figure 2; Teagle et al., 2006, 2012). The hole ended in a second screen of sheeted dykes (Figure 2).

The rocks of both dyke screens, as well as those from the base of the sheeted dyke complex, have granoblastic textures characterized by an assemblage of plagioclase, two pyroxenes and Fe-oxides (Koepke et al., 2008; Teagle et al., 2006, 2012). This assemblage is indicative of upper amphibolite to granulite-facies metamorphism, consistent with their positions at the top of the lower crust, the magmatic system of which served as a heat source (Koepke et al., 2008). The gabbroic rocks and granoblastic dykes are intruded by numerous cm-scale patches, veins and dykelets that range in composition from oxide gabbro and diorite to tonalite (Figure 2). These evolved rocks are generally medium-grained with granular textures, and commonly contain accessory phases such as apatite and zircon (Teagle et al., 2012). In contrast to the granoblastic textures of their host rocks, these intrusions retain igneous textures. They do, however, have high-temperature contacts with their host rocks, which indicates that they are late- to post-peak metamorphism (Teagle et al., 2012). The contacts of the patches with the granoblastic host rocks vary from moderately sharp and comb-textured to gradational; hence, the patches may comprise

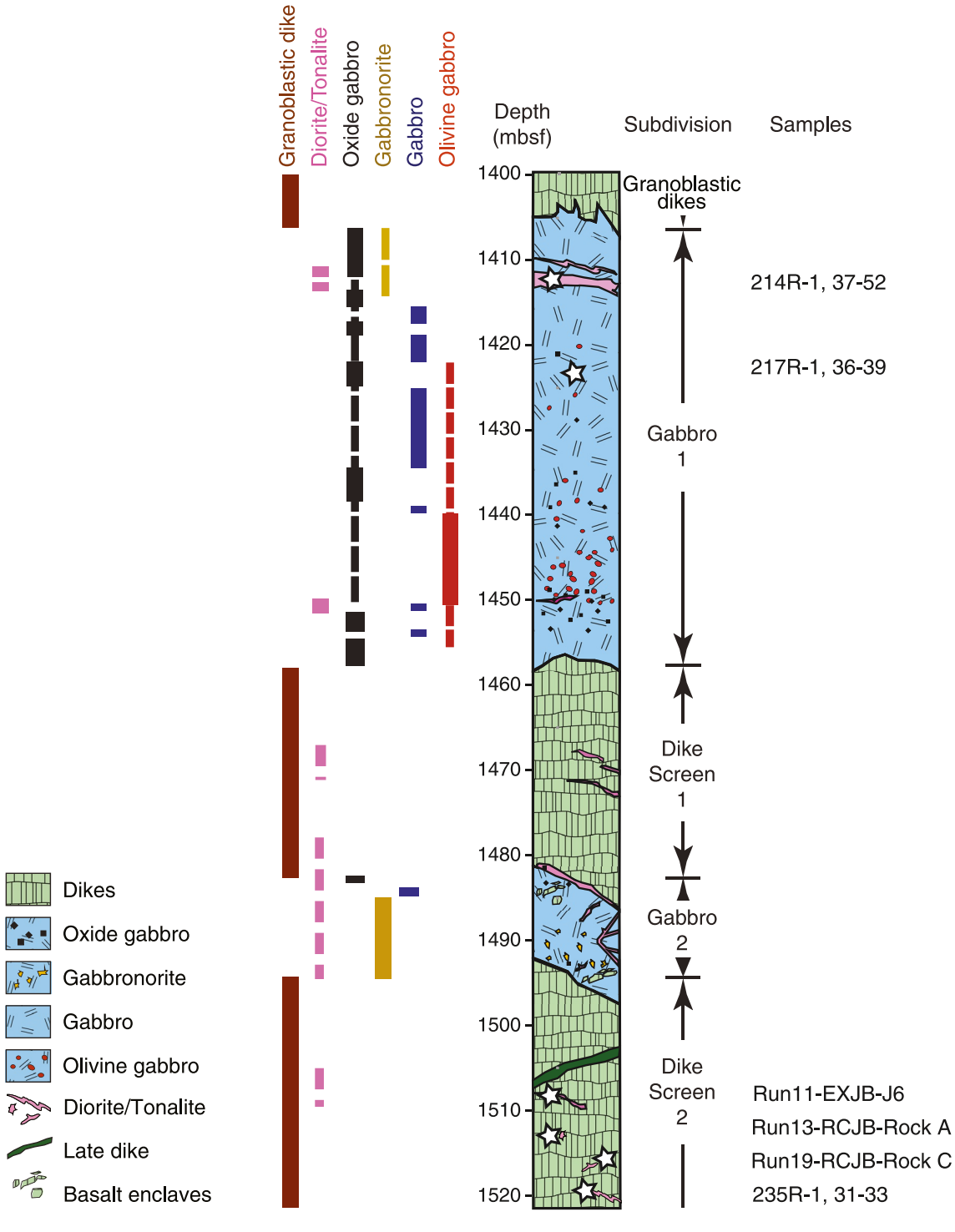

Figure 2. Igneous stratigraphy of the lower ~120 m of Hole 1256D, which recovered the transition from the upper crust to the lower crust. Samples studied in this paper are indicated by the white stars. Modified from Teagle et al. (2012).

both intrusions and segregations (Teagle et al., 2012). The relationships between the granoblastic dykes and the evolved intrusions within them have been the subject of recent interest. A number of observations have led to a model in which both the granoblastic textures and the intrusions are generated by partial melting of hydrothermally altered sheeted dykes during contact metamorphism (Erdmann et al., 2015, 2017; France et al., 2009, 2010;

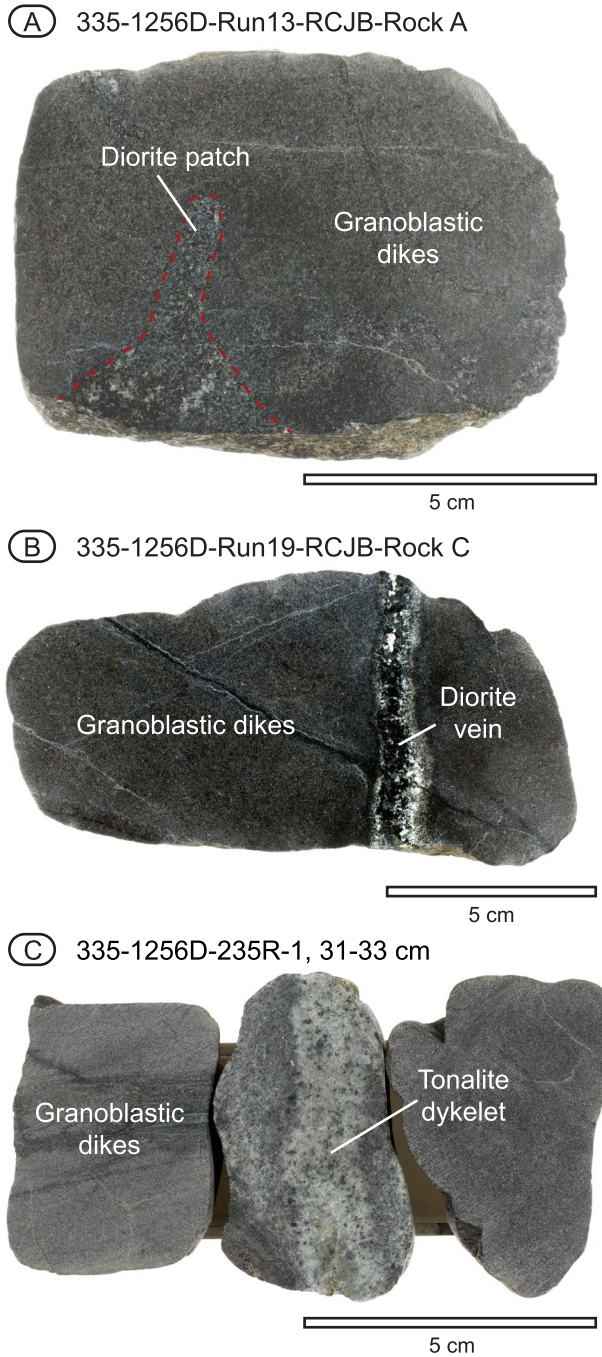

Figure 3. Igneous relationships of intrusive rocks in Dike Screen 2 sampled for geochronology. Intrusions include (a) diorite patch, (b) diorite vein, and (c) tonalite dykelet in granoblastic dike rocks.

Teagle et al., 2012; Zhang et al., 2017). These observations include a trend of depletion in incompatible element contents of the granoblastic dykes toward their contacts with the gabbroic rocks (Teagle et al., 2012), and the trace element distributions in the evolved intrusions (Zhang et al., 2017). This process has been studied experimentally, with the experiments reproducing both the nature of the granoblastic residue as well as the composition of the partial melts from hydrothermally altered dyke rock starting materials (Erdmann et al., 2015, 2017; Fischer et al., 2016; France et al., 2010). Hence, the recovered dyke-gabbro transition is a dynamic horizon, characterized by intrusion, metamorphism and partial melting.

We selected six samples recovered from Hole 1256D during IODP Expeditions 312 and 335 that span the igneous history of the section (Figure 2). These data supplement, and significantly expand upon, the geochronological data on three samples (two of Gabbro 1 and one of Gabbro 2) presented in Hayman et al. (2019). Hayman et al. (2019) relied mostly on relatively low-precision SIMS analysis but also provided higher precision ID-TIMS data for one Gabbro 1 sample. The latter data are directly comparable to those that we will present in this paper.

Within our data set, the main episode of crustal magmatism is represented by an oxide- and orthopyroxene bearing gabbro from Gabbro 1 (sample 312-1256D-217R-1, 36–39 cm). This sample is notably less patchy than most of Gabbro 1, suggesting it is predominantly comprised of the earlier, relatively primitive framework rather than any crystallization products of later and more evolved melts; hence, it maximizes the likelihood of dating the crystallization of the main Gabbro 1 magma, rather than any late-stage intrusive in it. The Gabbro 1 sample is supplemented by a sample of the <1 m thick quartz-rich oxide diorite that intrudes Gabbro 1 near its top (sample 312-1256D-214R-1, 37–52 cm). The oxide diorite locally has a comb structure defined by elongate plagioclase and likely magmatic amphibole, characteristic of fairly sharp but high-temperature intrusion into the Gabbro 1 host rock (Teagle et al., 2006). The remaining four samples represent various occurrences of evolved intrusive veins, dykelets and patches in Dyke Screen 2 (Figures 2 and 3). Three samples were taken from rocks that were recovered during cleaning operations in the hole, and derive from the borehole wall rather than drill core (for details, see Teagle et al., 2012). The exact origin and stratigraphic position of these rocks cannot be ascertained; however, the shipboard party considered it most likely that they were derived from near the bottom of the hole (Teagle et al., 2012). The first of these samples is 335-1256D-Run19-RCJB-Rock C, which is a prominent, cm-wide diorite vein with moderately sharp contacts with the granoblastic dykes (Figure 3b). The other two, samples 335-1256D-Run11-EXJB-J6 and 335-1256D-Run13-RCJB-Rock A, represent the evolved patches in Dyke screen 2 (Figure 3a), and are oxide-bearing diorite and oxide quartz diorite, respectively. Both have diffuse margins against their host granoblastic dykes. The last sample, 335-1256D-235R-1, 31–33 cm is a 2 cm wide tonalite dykelet cored from the bottom of the hole. It has fairly diffuse margins against the surrounding granoblastic dykes (Figure 3c), suggesting that it intruded when the dykes were at high temperature.

3. Methods

Samples were crushed using a steel jaw crusher and disk mill. The <500 μm fraction was processed using a Gemini table in order to extract a heavy mineral concentrate, which was further purified by passing through

di-iodomethane with a specific gravity of 3.3. The most magnetic material was extracted using a hand magnet and a Frantz magnetic separator. Zircons, typically in the form of crystal fragments, were hand-picked from the non-magnetic fraction for ID-TIMS analysis. Medial melt inclusions were common. After picking, the zircons were chemically abraded following a modified procedure to remove damaged parts of the crystal that were likely to have experienced open-system behavior. First, the zircons were thermally annealed at 900°C for 60 hr in quartz crucibles before being individually selected, photographed and loaded into FEP Teflon beakers. Zircons were then refluxed in 4 M HNO_3 on a hotplate at 120°C for >2 hr, followed by ultrasonic cleaning for at least 20 min. The zircon crystals were rinsed with acetone and 4 M HNO_3 and loaded into individual 300 µl FEP Teflon micro-capsules and leached in 29 M HF inside a Parr vessel (a self-sealing stainless-steel jacket) for 12 hr at 180°C. The zircons were rinsed with 4 M HNO_3 and refluxed in 6 M HCl at 120°C for 2–5 hr, before a final rinsing with 4 M HNO_3 several times.

The leached zircons and all total procedural blanks were spiked with mixed ^{205}Pb–^{233}U–^{235}U (ET535) EARTH-TIME tracer solution and dissolved in ~150 µl 29 M HF and trace HNO_3 in a Parr vessel at 220°C for ~60 hr. Complete dissolution was checked by visual inspection of some larger crystals and assumed for smaller grains, following the standard protocol for dissolution at NIGL. The solutions were dried down as fluorides and re-dissolved in 3 M HCl in a Parr vessel overnight at 180°C. U and Pb fractions were isolated by an HCl-based anion exchange procedure using Bio-Rad AG-1 resin in Teflon columns. Lead and U fractions were then recombined and dried down with ~10 µl of H_3PO_4 and subsequently loaded onto zone-refined Re filaments in a silica gel matrix to enhance ionization.

Isotope ratios were measured on a Thermo-Electron Triton TIMS. Lead was measured in the dynamic mode on a MassCom secondary electron multiplier; Pb mass bias corrections were made using a fractionation factor of 0.14 ± 0.02% amu-1 (1 sigma) for samples spiked using ET535. Dead-time and linearity of the secondary electron multiplier were monitored using repeated analyses of the standards NBS 982, NBS 981, and U 500. Uranium oxide (UO_2) was measured and corrected for isobaric interferences using an $^{18}O/^{16}O$ value of 0.00205 (IUPAC value and measured in-house at BGS; Condon et al., 2015; de Laeter et al., 2003). Uranium was measured in dynamic mode and a mass bias fractionation correction was calculated in real-time using the ^{233}U–^{235}U ratio of the ET535 tracer solutions. Corrections for the addition of Pb and U during the procedure (i.e., laboratory contamination) were made using the long-term measured isotopic composition and variability of blanks using an amount that is based upon contemporary total procedural blanks.

The U/Pb ratio for each analysis was determined via isotope dilution principles and the ET535 mixed ^{205}Pb-^{233}U–^{235}U tracer (Condon et al., 2015; McLean et al., 2015). A $^{238}U/^{235}U$ value of 137.818 was assumed (Hiess et al., 2012) and used in the data reduction algorithm (McLean et al., 2011). Following the approach of Hayman et al. (2019) and to facilitate the comparison of data between these two studies, ^{238}U-^{206}Pb dates were corrected for initial ^{230}Th disequilibrium using a Th/U[magma] value of 2.63. In presenting the data, we use the unit Ma to refer to dates, and Myr and kyr to describe duration.

4. Results

Zircons from Hole 1256D are dominated by euhedral, prismatic grains and grain fragments (Figure 4). The grains are up to several hundred µm long. In the diorite patches, where zircon is readily apparent in thin section, it is intergrown with amphibole, which forms a primary phase in these rocks, and plagioclase. This indicates that, in these samples, zircon crystallized cogenetically with the rock-forming silicate phases, consistent with the presence of primary Fe-Ti oxides and indicating that they are crystallization products of evolved melts.

The results of the U-Pb analyses are listed in Table S1 and illustrated in Figures 5–7. Overall, the Th-corrected zircon $^{206}Pb/^{238}U$ dates range from 14.56 to 15.31 Ma, with a single outlier at 15.82 Ma (Figure 5). All zircons except the 15.82 Ma outlier overlap concordia (Figure 6). 2σ errors on individual dates range from 0.02 to 1.03 Myr, with a median of 0.13 Myr, and show a negative power-law correlation with the ratio of radiogenic to common lead (Pb^*/Pb_c) (Figure 7a). Calculated zircon Th/U ratio range from 0.9 to 3.9, a range comparable to those reported in Hayman et al. (2019). Pb^*/Pb_c is highly variable, ranging from 0.15 to 12.59. In addition to precision reducing dramatically at low Pb^*/Pb_c, the $^{206}Pb/^{238}U$ dates of grains with low Pb^*/Pb_c (<0.5) are younger than those with higher Pb^*/Pb_c (Figure 7b). This is true even within individual samples, with dates for grains with low Pb^*/Pb_c deviating from those with higher Pb*/Pbc (Figure 7b). This indicates that those analyses

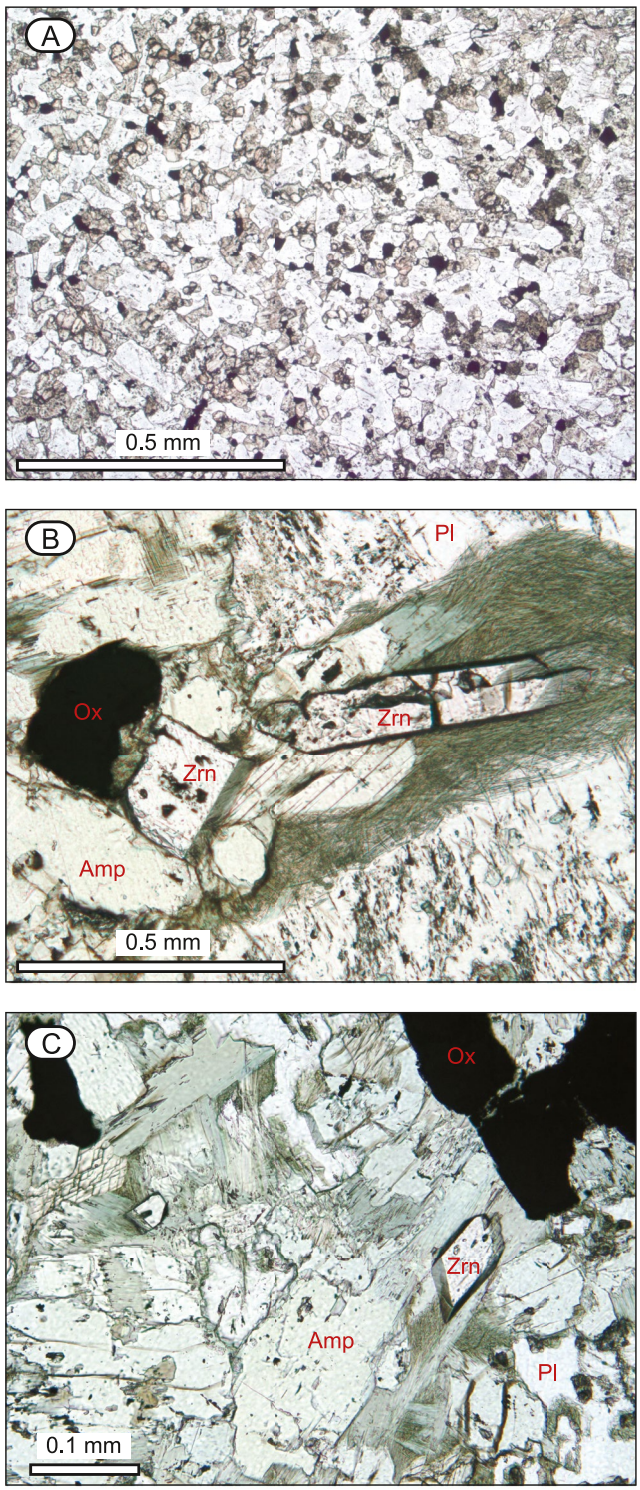

Figure 4. Photomicrographs of samples (a and b) 335-1256D-Run11-EXJB-J6 and (c) 335-1256D-Run13-RCJB-Rock A illustrating the nature of the granoblastic dykes (a) and the occurrence of zircon in diorite patches (b and c). Amp = amphibole; Pl = plagioclase; Ox = Fe-oxide; Zrn = zircon.

that are dominated by common lead are unlikely to represent the true crystallization age of these grains. We attribute this to inclusions that were observed prior to leaching and not fully removed during chemical abrasion, and that crystallization ages are likely to be best preserved in those grains with high Pb^*/Pb_c. For this reason, we do not incorporate grains with Pb^*/Pb_c below 0.5 in the data presentation and discussion below.

The sample representing Gabbro 1 (312-1256D-217R-1, 36–39 cm) yielded single grain $^{206}Pb/^{238}U$ dates of 15.25–15.09 Ma (n = 9; Figures 5 and 6). All grains are mutually within error, and the population has a mean squared weighted deviation (MSWD) of 0.68. This is consistent with a single population origin for zircon within this sample. These single grain dates, as well as their weighted mean (15.17 ± 0.03 Ma), are in agreement with the ID-TIMS data for Gabbro 1 reported by Hayman et al. (2019) (range 15.24–15.12 Ma; weighted mean 15.19 ± 0.04 Ma). They also overlap with the SIMS date for Gabbro 2 (15.23 ± 12; Hayman et al., 2019). Although caution has to be exercised when comparing zircon dates obtained using different methods, this suggests that Gabbro 1 and 2 crystallized in close temporal proximity.

The oxide diorite crosscutting Gabbro 1 (sample 312-1256D-214R-1, 37–52 cm) contains a population of zircons (n = 9) with $^{206}Pb/^{238}U$ dates of 15.25–15.06 Ma (Figures 5 and 6); they are mutually within error (MSWD = 0.98). In addition, it contains a single outlier at 15.82 Ma; this grain has the highest Pb^*/Pb_c of any zircon analyzed in this study (Figure 7).

The diorite vein crosscutting Dyke Screen 2 (sample 335-1256D-Run19-RCJB-Rock C), like Gabbro 1 and its crosscutting oxide diorite, define a statistically uniform population at the current level of precision, with a range in dates of 15.22–14.94 Ma (n = 8; MSWD = 1.23; Figures 5 and 6). The tonalite dykelet crosscutting Dyke Screen 2 (sample 335-1256D-235R-1, 31–33 cm), on the other hand, does not appear to comprise a single statistical population: although its range in dates is very similar to the other dates rock units (15.12–15.29 Ma), two high-precision dates (2σ errors of 0.04 and 0.05 Ma) are not within error of each other, differing in age by a minimum of 0.02 Myr. This is also reflected by the relatively high MSWD for this sample (2.48; n = 7).

One of the two dated evolved plutonic patches in Dyke Screen 2, sample 335-1256D-Run11-EXJB-J6, shows very similar results to Gabbro 1 and the crosscutting units: its single grain dates range from 15.31 to 15.14 Ma, and all dates are within error, with an MSWD of 1.19 for the population as a whole (n = 8; Figures 5 and 6). The second patch (sample 335-1256D-Run13-RCJB-Rock A), however, deviates from all of the other dated units: its two zircons with Pb*/Pbc>0.5 both have dates of 14.94 Ma (Figures 5 and 6). The significance of this observation will be discussed below.

5. Discussion

5.1. Significance of Hole 1256D Zircon Dates

To date, significant variations in zircon dates of both individual grains and individual samples have been observed at (ultra)slow- and fast-spreading ridges, suggesting that crustal accretion is a protracted process (Baines et al., 2009; Grimes et al., 2008; C. J. Lissenberg et al., 2009; Rioux, Lissenberg, et al., 2012; Schwartz et al., 2005). However, at the high spreading rates prevalent during the formation of the section drilled in Hole 1256D, the crust is carried away from the spreading center very rapidly. As a result,

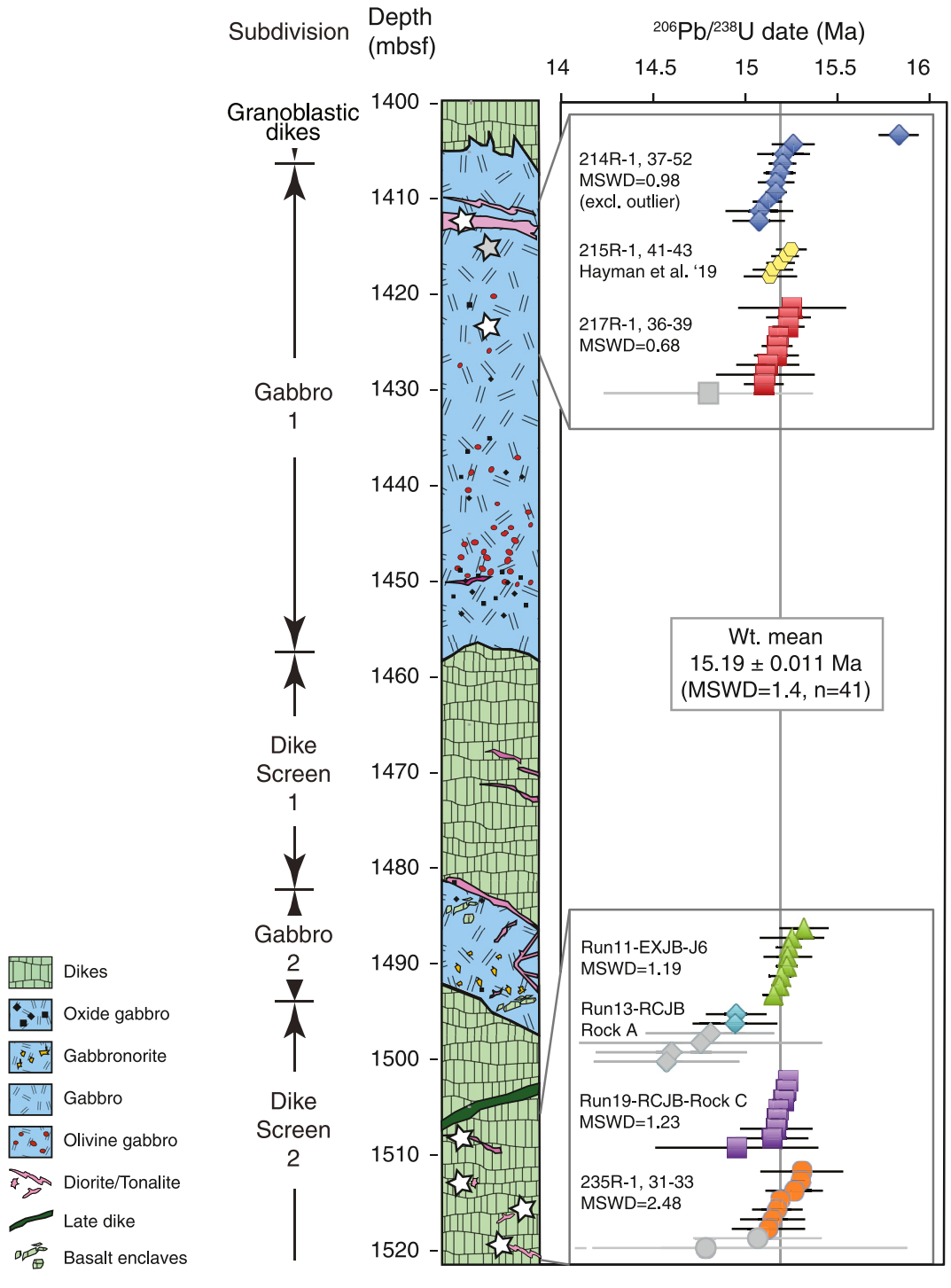

Figure 5. Zircon U-Pb results as a function of stratigraphic depth in Ocean Drilling Program Hole 1256D. The zircon U-Pb TIMS data for the single sample presented by Hayman et al. (2019) are included for comparison. Light gray datapoints are those with high Pb^*/Pb_c, and are excluded from the interpretations and discussion (see text for details). The stratigraphic log after Teagle et al. (2012).

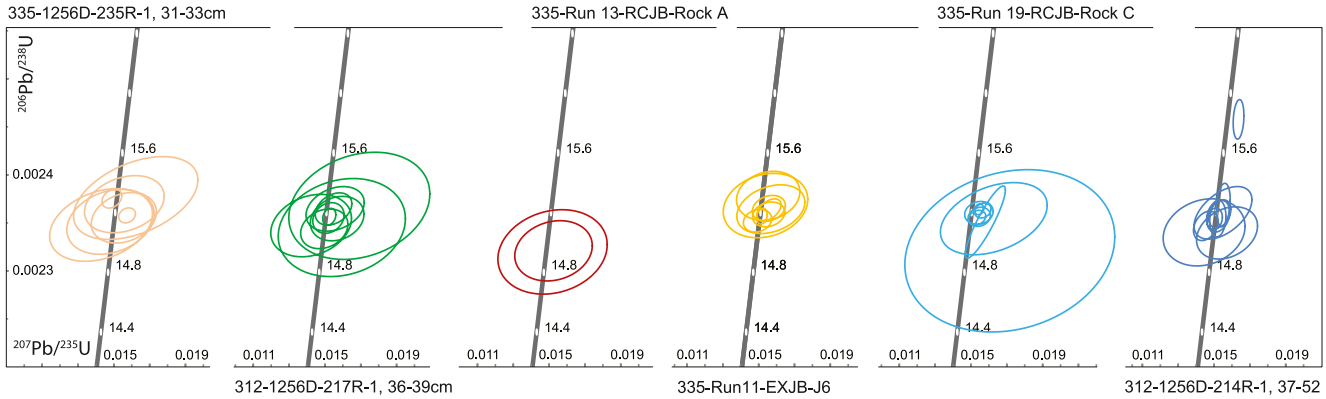

Figure 6. Concordia plots for zircons from Ocean Drilling Program Hole 1256D.

crustal accretion is expected to be rapid. Here, we examine the significance of the zircon dates of Hole 1256D, as well as the time span of magmatism that they record for the section.

It is striking that, with the exception of sample 335-1256D-Run13-RCJB-Rock A and the single zircon outlier in the oxide diorite at the top of the section (15.82 Ma), all samples show very similar dates. To test whether there is any statistically significant difference in dates within this population overall, we have calculated the MSWD of the full zircon population from all samples except 335-1256D-Run13-RCJB-Rock A, and excluding the 15.82 Ma outlier. The resulting MSWD is 1.4 (n = 41). This is consistent with the notion that, statistically, all of these samples behave as a single population, the weighted mean date of which is 15.19 ± 0.011 Ma. As pointed out by Hayman et al. (2019), this date fits well with the magnetic anomalies of the area: Hole 1256D was sited just east of the marine magnetic anomaly transition 5Bn-5Br, which corresponds to an age of ~15.1 Ma using the time scale of Cande and Kent (1995) (Wilson, Hallenborg, et al., 2003; Figure 1). However, it should be noted that the weighted mean of 15.19 Ma is only significant if the population forms a normally distributed dataset defined by analytical error around a single crystallization date. There are a number of indications that this condition is not normally met for zircon in oceanic plutonic rocks. The first, and most direct, is that different zircons from the same sample are not always within error (C. J. Lissenberg et al., 2009; Rioux, Lissenberg, et al., 2012; Schwartz et al., 2005). This is also the case for one of the samples under consideration here: two single-grain zircon dates of the tonalite dykelet crosscutting Dyke Screen 2 (sample 335-1256D-235R-1, 31–33 cm) are not within error of one another, requiring a minimum duration of crystallization of 0.02 Myr. Furthermore, the youngest and oldest grain from the main population, which occur in samples sample 312-1256D-214R-1, 37–52 cm and

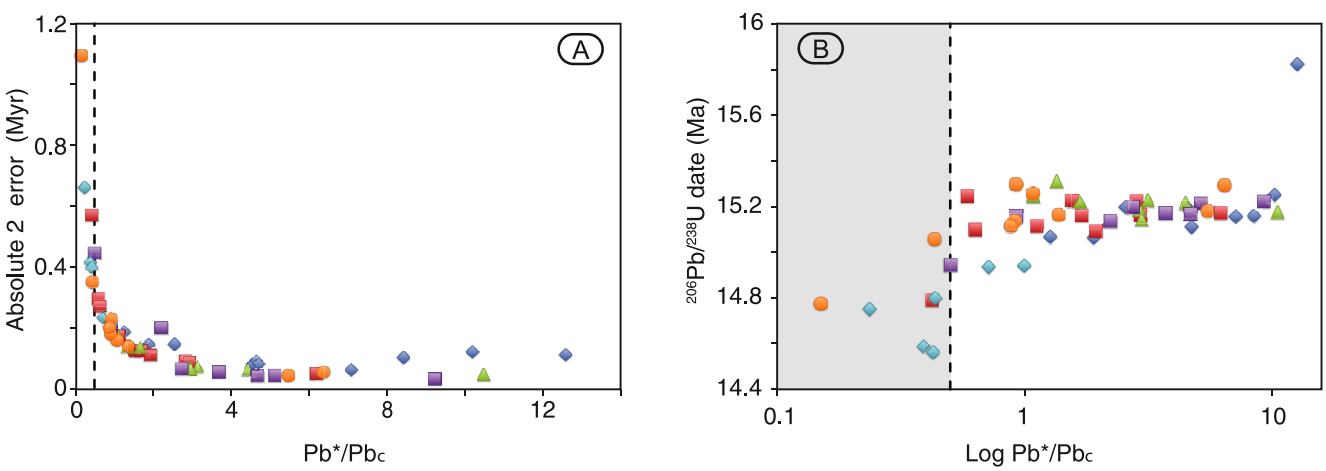

Figure 7. (a) Relationship between 2σ error of $^{206}Pb/^{238U}$ U-Pb dates and the ratio of radiogenic to common lead (Pb^*/Pb_c). (b) Relationship between individual zircon $^{206}Pb/^{238}U$ U-Pb dates and Pb^*/Pb_c. At low Pb^*/Pb_c, precision reduces dramatically, and dates become anomalously young compared to zircons from the same sample with higher Pb^*/Pb_c. Consequently, data with Pb^*/Pb_c below 0.5 (gray field) have not been used in the interpretations (see text for discussion). Data points are color coded by the sample, using the same color scheme as in Figure 5.

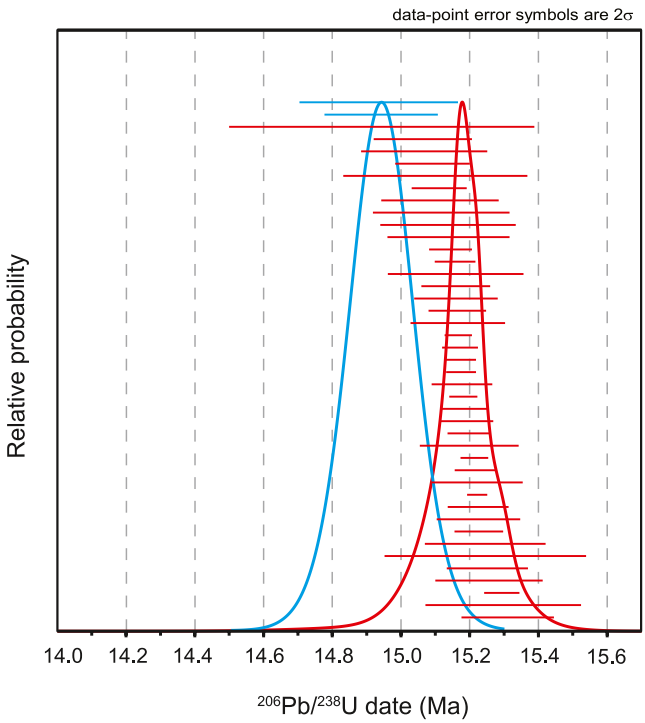

Figure 8. Ranked $^{206}Pb/^{238U}$ dates for all zircons dated in this study, separated into the main population (red) and those of sample 1256D-Run13-RCJB-Rock A (blue), with their respective probability density curves superimposed. Errors on dates are 2σ.

335-1256D-235R-1, 31–33 cm, respectively, require a minimum of 0.05 Myr crystallization (taking into account their respective errors). The second indication that oceanic zircons may not represent single crystallization episodes is that they tend to preserve a range of trace element concentrations, even within individual samples (Grimes et al., 2009). This is inconsistent with the crystallization of zircon at a single point in time; instead, it appears to crystallize over an extended part of the liquid line of descent of its parental magma (C. J. Lissenberg et al., 2009). On the basis of these two observations, oceanic zircons are not expected to form uniform populations with a normal distribution related to analytical error. If so, weighted means do not represent statistically valid dates. Nonetheless, at the current level of precision, the large majority of zircons dated in this study appear to define a single population. In Figure 8, we examine the distribution of dates of this population. Overall, the distribution is not unlike a normal distribution, albeit with a slight skew to older dates. Given the low MSWD of this population, as well as its distribution (Figure 8), we consider 15.19 Ma to be the best estimate of the main episode of zircon crystallization in this section. The minimum spread of 0.05 Myr between different zircons from this population indicates that the main crystallization episode likely spanned some tens of thousands of years.

Both dates (14.94 Ma) for one of the patches in Dyke Screen 2 (sample 335-1256D-Run13-RCJB-Rock A) are on the young end of the spectrum defined by the other samples: they are younger than all of the other zircon grains dated in this study (Figure 8). As a result, when including these two grains in the main population of zircons dated in this study, its MSWD increases from 1.4 to 2.0. This indicates that, statistically, they are unlikely to form part of the main population. Furthermore, the patch is the only sample for which no dates fall in the 15.0–15.30 Ma range, and the most precise single-grain date for this patch (14.94 ± 0.17 Ma, 2σ) is outside the error of 39% of all of the other dates presented in this study. The difference in dates between the main population and the patch is illustrated by their probability density distributions, which show only a small amount of overlap (Figure 8). The most likely interpretation, therefore, is that this patch is younger than the other units. It is not possible, however, to quantify just how much younger: the 14.94 Ma dates are within error of the younger dates of the main population, and whether the main population can be treated as a single crystallization event with a geologically significant mean date is uncertain (see above). Nonetheless, a maximum age difference is provided by the difference between the 15.19 Ma mean of the main population and the 14.94 Ma dates of the younger zircons. This maximum, which is 0.25 Myr, makes the assumption that the mean date of the main population is geologically significant, and ignores the errors on the dates. In reality, some of the younger zircons of the main population may have crystallized after 15.9 Ma, and the two dates from sample 335-1256D-Run13-RCJB-Rock A overlap within error with the majority of grains from the main population, making it likely that the actual age difference is smaller than 0.25 Myr.

The most remarkable data point is the 15.82 ± 0.11 Ma (2σ) Ma outlier in sample 312-1256D-214R-1, 37–52 cm. Taking into account their respective errors, it is at least 0.51 Myr older than the weighted mean of the main population of zircons (15.19 ± 0.011 Ma). One possible explanation is that the anomalously old zircon is derived from the drilling mud used during drilling of the hole. Sepiolite, one of the types of mud used during scientific ocean drilling, contains abundant zircons with a wide range of ages (2–2889 Ma; Andrews et al., 2016). Of particular note is that the age distribution of this sepiolite mud shows a secondary peak at 15.7 ± 0.2 Ma, which overlaps with the outlier in our data. However, the type of drilling mud used on Expedition 312 was not recorded, so it is not clear whether sepiolite was in fact used. Further, the Th/U of 3.7 of the 15.82 Ma outlier is higher than those of the majority of sepiolite zircon. Hence, although we cannot rule out contamination, it appears unlikely that the outlier is related to drilling mud. Older outliers have been found in oceanic plutonic rocks before: Schwartz et al. (2005) describe zircon cores ~1.5 Myr older than their surrounding rims in gabbroic rocks from the Atlantis Bank massif in the Indian Ocean. Since the zircon rim dates overlap with the magnetic age of the crust, the cores were interpreted as inherited fragments of zircon formed prior to

the main episode of crustal magmatism. At (ultra)slow spreading rates prevalent at the Southwest Indian Ridge this is a plausible scenario since the lithosphere is significantly thicker than the crust (e.g., Schlindwein & Schmid, 2016). This situation leads to the potential for crystallization in the deeper parts of the (mantle) lithosphere, and the subsequent upward transport of the resulting plutons to the shallow part of the lithosphere by corner flow. There, the main axial magmatism has the potential to assimilate zircons from the older plutons that initially crystallized at depth (Schwartz et al., 2005). Anomalously old zircons have also been found in plutonic rocks from the Oman ophiolite (Rioux, Bowring, et al., 2012). These zircons occur as individual grains that are up to 16.8 Myr older than the young cluster of zircons interpreted to reflect the crystallization age of the rocks (Rioux, Bowring, et al., 2012). The origin of these outliers remains enigmatic: they may relate to the propagation of the spreading ridge into older crust, or may represent zircon grains that were derived from subducted material (Rioux, Bowring, et al., 2012). For the 15.82 Ma outlier at Hole 1256D, two of these three possible explanations are unsatisfactory. Unlike Oman, a contribution from subducted material is unlikely as the Hole 1256D section did not form in the vicinity of a subduction zone. Similarly, because of the high rates of heat advection from the upwelling mantle and the large volumes of melt delivered to the crust, superfast-spreading ridge axes should not have thick lithosphere. The third possibility is that the zircon grain is inherited when the main magmatic pulse intrudes into older crust in a propagating rift or overlapping spreading center. Given the half-spreading rate on the Cocos plate during the formation of the Hole 1256D section (~96 mm/yr; Wilson, 1996), 0.51 Myr of spreading corresponds to 49 km of crustal growth across-axis. Hence, the outlier could represent an inherited relic of crust that was subject to a propagating rift when it was 49 km off-axis. This is within the range of offsets recorded by current overlapping spreading centers at the Pacific, which can be up to 120 km, particularly where spreading rates are very fast (Martínez et al., 1997). However, the southernmost segment of the Pacific-Cocos Ridge had a length of at least 400 km, with no apparent evidence for significant ridge axial discontinuities. Furthermore, the magnetic anomalies around Hole 1256D, which have a spatial resolution of 1 km near the Hole and 5 km around it, show no indications for any offsets (Wilson, Hallenborg, et al., 2003). Hence, there is little supporting evidence for a propagating rift origin of the outlier. We conclude that its origin remains enigmatic.

5.2. Implications for Oceanic Crustal Accretion at Hole 1256D

The dates presented in this paper, supplemented by those of Hayman et al. (2019), enable us to place constraints on the history of crustal accretion preserved in Hole 1256D. The main episode of zircon crystallization occurred around 15.19 Ma, and likely lasted at least 0.05 Myr. Given the half-spreading rate of the Cocos plate at the time of accretion of the section in the Miocene (96 mm/yr), this time span translates to 4.8 km of spreading. Although there are currently no mid-ocean ridges on Earth with spreading rates as high as the Pacific-Cocos ridge during the Miocene, seismic data from the fast-spreading East Pacific Rise provide constraints on the width of the magmatic system beneath the ridge axis. Seismic tomography and seafloor compliance data have shown that a low-velocity zone, comprising a region of partial melt, occupies most of the lower crust (Crawford et al., 1999; Crawford & Webb, 2002; Dunn et al., 2000). It is generally ~8–10 km wide, and is overlain by a narrower lens with higher melt proportions (Sinton & Detrick, 1992). This axial melt lens or AML is observed along the majority of the East Pacific Rise, and is generally <1 km but up to 4 km wide (Detrick et al., 1993; Mutter et al., 1995; Vera et al., 1990). Further constraints on the width of the crustal accretion zones come from the lava: although most lava along the East Pacific Rise erupt in the relatively narrow (hundreds of meters) axial summit through, volcanic rocks continue to erupt up to four km away from the ridge axis (Goldstein et al., 1994; Sims et al., 2003). All of these existing constraints fit well with the inference from the zircon data that the main episode of crystallization occurred over a time span of 0.05 Myr.

During this main episode of crustal accretion, both Gabbro 1 and the oxide quartz diorite that cuts it was formed. Gabbro 1's occurrence as an ~50 m thick body within the lower part of the sheeted dyke complex suggests that at the time of its intrusion, it formed the type of melt body that is imaged geophysically as the AML. Although its lateral extent is unknown, its thickness, coupled with the fact that it is composite lithologically, is consistent with what would be expected from an AML. If so, Gabbro 1 marks the highest level AML of what would be a series of AMLs over the course of the crustal accretion history of the section, consistent with the notion that the AML horizon is dynamic and may migrate vertically over hundreds of meters (France et al., 2009; Hooft et al., 1997). Given the overlap in dates, it is likely that Gabbro 2 formed around a similar time as Gabbro 1, marking the emplacement of another melt lens within the deep portion of the sheeted dyke complex.

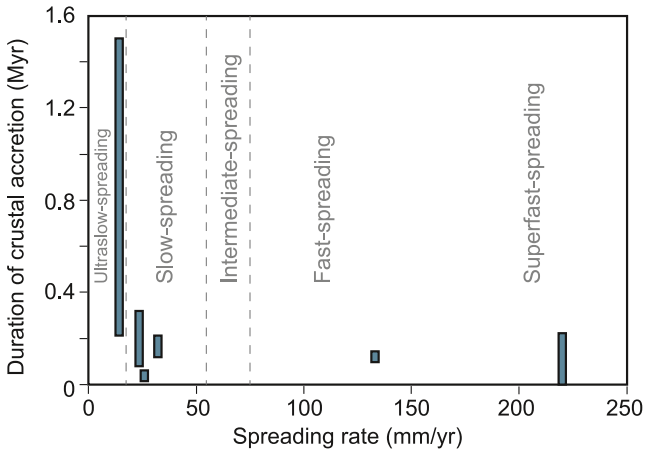

Figure 9. Duration of oceanic crustal accretion as revealed by zircon geochronology as a function of spreading rate. Vertical extent of the various bars represent either the range present in different studies from the same location (e.g., Atlantis Bank [15 mm/yr]), or the uncertainties on the duration as quoted in the original papers (e.g., Atlantis Massif [24 mm/yr], Vema [32 mm/yr], Hess Deep [133 mm/yr], this study [220 mm/yr]). Data from Baines et al. (2009); Grimes et al. (2011); Grimes et al. (2008); C. J. Lissenberg et al. (2009); Rioux et al. (2016); Rioux, Lissenberg, et al. (2012); Schwartz et al. (2005) and this paper. Boundaries between different classes of ocean ridges from Dick et al. (2003).

The diorite vein, tonalite dykelet and one of the diorite patches in the granoblastic dykes of Dyke Screen Two crystallized within the same time window as the gabbros. These veins and patches have been attributed to partial melting of the base of the sheeted dykes as a result of contact metamorphism by the main magmatic system below (Erdmann et al., 2015, 2017; France et al., 2009, 2010; Teagle et al., 2012; Zhang et al., 2017). The fact that the zircon dates of the diorite vein, the tonalite dykelet, and one of the diorite patches are indistinguishable from that of Gabbro 1, and that this main population of dates is in keeping with the magnetic age for the crust, is consistent with this scenario: both Gabbro 1 and the partial melt in the metamorphosed granoblastic dykes are formed as part of the main axial sequence. The second diorite patch in the granoblastic dykes, however, appears to postdate this axial sequence. Although it is not possible to quantify the age difference, the offset is <0.25 Myr, which equates to <24 km of spreading. Hence, this diorite may represent an off-axis intrusion. Off-axis sills have been documented in seismic studies, extending up to eight km from the axial low-velocity zone (Canales et al., 2012). Furthermore, sills at the Moho have been found up to 22 km off-axis (Garmany, 1989). The lava stratigraphy of Hole 1256D is capped by a 75 m thick lava pond, which has been interpreted to have erupted off-axis (Crispini et al., 2006; Tartarotti et al., 2009; Tominaga & Umino, 2010; Wilson, Teagle, et al., 2003). There is thus a record of off-axis magmatism at fast-spreading ridges in general, and at 1256D in particular. Hence, it is possible that the diorite patch reflects the late-stage delivery of melts to the crust as it is carried off-axis. In this scenario, it would represent an intrusion of melt that underwent significant amounts of differentiation from off-axis basalt. However, the diffuse margin of the patch with the granoblastic dykes suggests that the host rocks were still at elevated temperatures when the patch intruded, which suggests that either the section remained hot for an extended period of time, or that the age difference between the patch and main population is relatively small. Alternatively, we cannot completely rule out that the patch may be of the same age as the other intrusions in the granoblastic dykes: although an age difference appears to be present (Figures 5 and 8), the associated errors allow for zircon from the patch to have crystallized synchronously to at least some zircons of the main population.

5.3. Time Span of Crustal Accretion Across the Spreading Rate Spectrum

With the addition of superfast-spreading crust to the global zircon geochronology dataset for oceanic crust, there are now data on the duration of crustal accretion across nearly the full range of spreading rates of the global mid-ocean ridge system. In Figure 9, we examine the pattern that emerges. As noted before (Grimes et al., 2011; Rioux, Lissenberg, et al., 2012), there appears to be little difference in the duration of crustal accretion between slow- and fast-spreading ridges, with most sites recording periods of ∼100–300 kyr. Our new data suggest that this observation extends to superfast-spreading ridges. This observation likely reflects the competing effects of the longevity of the magmatic system on the one hand and the rate of crustal transport off-axis on the other (Rioux, Lissenberg, et al., 2012). Faster spreading ridges feature more robust—and hence longer-lived—magmatic systems but are carried off-axis rapidly. Magmatic events at lower-spreading ridges may be shorter-lived, but the crust remains in the axial valley for longer periods of time. The net effect is that the total duration recorded by the zircon record is similar. Ultraslow-spreading crust may be an exception to this: the 1.5 Myr span recorded by zircon at the Southwest Indian Ridge far exceeds that observed elsewhere (Figure 9). This likely reflects the fact that the ultraslow-spreading lithosphere is substantially thicker than slow- to fast-spreading ridge lithosphere (Bennett et al., 2019; Schlindwein & Schmid, 2016). This is because mantle upwelling is slow, leading to reduced melt production and heat advection. The cool thermal structure results in thick lithosphere, with earthquake data indicating that the brittle lithosphere may extend to 35 km depth (Schlindwein & Schmid, 2016). This promotes initial crystallization of melts deep in the mantle lithosphere, evidence for which has recently been found in the melt inclusion record (Bennett et al., 2019). The subsequent upward transport of these plutons by corner flow, and the intrusion of melts into them at shallower levels, accounts for the extended time span of zircon crystallization (Schwartz et al., 2005). Although the lithosphere at slow-spreading ridges may locally also be thicker than the

magmatic crust (Cannat, 1996), crystallization depths of plutons are thought to be in the order of ∼6–7 km (Grimes et al., 2011; C. J. Lissenberg et al., 2016; Schoolmeesters et al., 2012), which is insufficient to lead to the extended periods of accretion recorded at the Southwest Indian Ridge. Hence, there appears to be a transition between very long (up to 1.5 Myr) duration of crustal accretion at ultraslow-spreading ridges characterized by thick lithosphere, to ∼100–300 kyr periods at slow-to superfast-spreading ridges.

6. Conclusions

Zircon U-Pb geochronology of plutonic rocks recovered from ODP Hole 1256D, which formed during an episode of superfast spreading at the Pacific-Cocos plate boundary, has revealed the following:

1. The main episode of crustal accretion occurred around 15.19 Ma, which is agreement with the seafloor age as estimated from magnetic anomalies. This episode likely spanned some tens of thousands of years and formed the main axial sequence. This comprises intrusions of gabbro into the base of the sheeted dyke complex as well as the formation and crystallization of partial melts of the deep part of the sheeted dykes.
2. One sample apparently postdates this main episode. Although we cannot quantify the age difference, it was most likely less than 0.25 Myr. This sample may represent an off-axis intrusion, although, based on the uncertainties of both the main population and the dates of the younger sample, we cannot rule out that it formed as part of the axial suite.
3. The time span of crustal accretion of oceanic crust is similar (∼100–300 kyr) across large parts of the spreading rate spectrum from slow- to superfast-spreading ridges, but may be substantially longer (up to 1.5 Myr) at ultraslow-spreading ridges characterized by thick lithosphere.

Data Availability Statement

Data can be accessed at the UK National Geoscience Data Centre (J. Lissenberg et al., 2023).

Acknowledgments
We thank the captain, crew and science parties of the four (I)ODP expeditions at Site 1256, whose tireless work has enabled significant new insights into oceanic crustal processes. CJL's participation in IODP Expedition 335 was funded by NERC Grant NE/J005592/1. Geochronology was funded by NERC Isotope Geosciences Facility Grant IP-1276-1111 to CJL. This research used samples and/or data provided by the Integrated Ocean Drilling Program (IODP). Adrian Wood and Nicola Atkinson provided technical assistance with the U-Pb zircon dating. We would like to thank reviewers Axel Schmitt and Joshua Schwartz for their helpful comments and suggestions. This is Cardiff EARTH CRediT Contribution 18.

References

Andrews, G. D., Schmitt, A. K., Busby, C. J., Brown, S. R., Blum, P., & Harvey, J. (2016). Age and compositional data of zircon from sepiolite drilling mud to identify contamination of ocean drilling samples. *Geochemistry, Geophysics, Geosystems*, *17*(8), 3512–3526. https://doi.org/10.1002/2016gc006397

Baines, A. G., Cheadle, M. J., John, B. E., Grimes, C. B., Schwartz, J. J., & Wooden, J. L. (2009). SHRIMP Pb/U zircon ages constrain gabbroic crustal accretion at Atlantis Bank on the ultraslow-spreading Southwest Indian Ridge. *Earth and Planetary Science Letters*, *287*(3–4), 540–550. https://doi.org/10.1016/j.epsl.2009.09.002

Baines, A. G., Cheadle, M. J., John, B. E., & Schwartz, J. J. (2008). The rate of oceanic detachment faulting at Atlantis Bank, SW Indian Ridge. *Earth and Planetary Science Letters*, *273*(1–2), 105–114. https://doi.org/10.1016/j.epsl.2008.06.013

Bennett, E. N., Jenner, F. E., Millet, M.-A., Cashman, K. V., & Lissenberg, C. J. (2019). Deep roots for mid-ocean-ridge volcanoes revealed by plagioclase-hosted melt inclusions. *Nature*, *572*(7768), 235–239. https://doi.org/10.1038/s41586-019-1448-0

Canales, J. P., Carton, H., Carbotte, S. M., Mutter, J. C., Nedimovic, M. R., Xu, M., et al. (2012). Network of off-axis melt bodies at the East Pacific Rise. *Nature Geoscience*, *5*(4), 279–283. https://doi.org/10.1038/ngeo1377

Cande, S. C., & Kent, D. V. (1995). Revised calibration of the geomagnetic polarity timescale for the Late Cretaceous and Cenozoic. *Journal of Geophysical Research*, *100*(B4), 6093–6095. https://doi.org/10.1029/94jb03098

Cann, J. R., Blackman, D. K., Smith, D. K., McAllister, E., Janssen, B., Mello, S., et al. (1997). Corrugated slip surfaces formed at ridge-transform intersections on the Mid-Atlantic Ridge. *Nature*, *385*(6614), 329–332. https://doi.org/10.1038/385329a0

Cannat, M. (1993). Emplacement of mantle rocks in the seafloor at mid-ocean ridges. *Journal of Geophysical Research*, *98*(B3), 4163–4172. https://doi.org/10.1029/92jb02221

Cannat, M. (1996). How thick is the magmatic crust at slow spreading oceanic ridges. *Journal of Geophysical Research*, *101*(B2), 2847–2857. https://doi.org/10.1029/95jb03116

Cannat, M., Chatin, F., Whitechurch, H., & Ceuleneer, G. (1997). Gabbroic rocks trapped in the upper mantle at the Mid-Atlantic Ridge. In J. A. Karson, M. Cannat, D. J. Miller, & D. Elthon (Eds.), *Ocean Drilling Program, Scientific Results* (pp. 243–264).

Cannat, M., Sauter, D., Mendel, V., Ruellan, E., Okino, K., Escartin, J., et al. (2006). Modes of seafloor generation at a melt-poor ultraslow-spreading ridge. *Geology*, *34*(7), 605–608. https://doi.org/10.1130/G22486.22481

Carbotte, S., Mutter, C., Mutter, J., & Ponce-Correa, G. (1998). Influence of magma supply and spreading rate on crustal magma bodies and emplacement of the extrusive layer: Insights from the East Pacific Rise at lat 16°N. *Geology*, *26*(5), 455–458. https://doi.org/10.1130/0091-7613(1998)026<0455:iomsas>2.3.co;2

Carbotte, S. M., Marjanovic, M., Carton, H., Mutter, J. C., Canales, J. P., Nedimovic, M. R., et al. (2013). Fine-scale segmentation of the crustal magma reservoir beneath the East Pacific Rise. *Nature Geoscience*, *6*(10), 866–870. https://doi.org/10.1038/ngeo1933

Chen, Y. J. (1992). Oceanic crustal thickness versus spreading rate. *Geophysical Research Letters*, *19*(8), 753–756. https://doi.org/10.1029/92gl00161

Condon, D. J., Schoene, B., McLean, N. M., Bowring, S. A., & Parrish, R. R. (2015). Metrology and traceability of U–Pb isotope dilution geochronology (EARTHTIME Tracer Calibration Part I). *Geochimica et Cosmochimica Acta*, *164*, 464–480. https://doi.org/10.1016/j.gca.2015.05.026

Conference Participants. (1972). Penrose Field Conference: Ophiolites. *Geotimes*, *17*, 24–26.

Cooper, K. M. (2007). Data report: Trace element analyses in wholerock basement samples, site 1256, ODP Leg 206. In D. A. H. Teagle, D. S. Wilson, G. A. Acton, & D. A. Vanko (Eds.), *Proceedings of the ODP, Scientific Results* (206th ed., pp. 1–10). Ocean Drilling Program.

Crawford, W. C., & Webb, S. C. (2002). Variations in the distribution of magma in the lower crust and at the Moho beneath the East Pacific Rise at 9°–10°N. *Earth and Planetary Science Letters*, *203*(1), 117–130. https://doi.org/10.1016/s0012-821x(02)00831-2

Crawford, W. C., Webb, S. C., & Hildebrand, J. A. (1999). Constraints on melt in the lower crustal and Moho at the East Pacific Rise, 9°48'N, using seafloor compliance measurements. *Journal of Geophysical Research, B, Solid Earth and Planets*, *104*(B2), 2923–2939. https://doi.org/10.1029/1998jb900087

Crispini, L., Tartarotti, P., & Umino, S. (2006). Microstructural features of a subaqueous lava from basaltic crust off the East Pacific Rise (ODP Site 1256, Cocos Plate). *Ofioliti*, *31*, 117–127.

de Laeter, J. R., Böhlke, J. K., De Bièvre, P., Hidaka, H., Peiser, H. S., Rosman, K. J. R., & Taylor, P. D. P. (2003). Atomic weights of the elements. Review 2000 (IUPAC Technical Report). *Pure and Applied Chemistry*, *75*(6), 683–799. https://doi.org/10.1351/pac200375060683

Detrick, R. S., Harding, A. J., Kent, G. M., Orcutt, J. A., Mutter, J. C., & Buhl, P. (1993). Seismic structure of the Southern East Pacific Rise. *Science*, *259*(5094), 499–503. https://doi.org/10.1126/science.259.5094.499

Detrick, R. S., Mutter, J. C., Buhl, P., & Kim, I. I. (1990). No evidence from multichannel reflection data for a crustal magma chamber in the MARK area on the Mid-Atlantic Ridge. *Nature*, *347*(6288), 61–64. https://doi.org/10.1038/347061a0

Dick, H. J. B., Bryan, W. B., & Thompson, G. (1981). Low-angle faulting and steady-state emplacement of plutonic rocks at ridge-transform intersections. *Eos, Transactions American Geophysical Union*, *62*, 406.

Dick, H. J. B., Lin, J., & Schouten, H. (2003). An ultraslow-spreading class of ocean ridge. *Nature*, *426*(6965), 405–412. https://doi.org/10.1038/nature02128

Dunn, R. A., Toomey, D. R., & Solomon, S. C. (2000). Three-dimensional seismic structure and physical properties of the crust and shallow mantle beneath the East Pacific Rise at 9°30′N. *Journal of Geophysical Research*, *105*(B10), 23537–23555. https://doi.org/10.1029/2000jb900210

Erdmann, M., Fischer, L. A., France, L., Zhang, C., Godard, M., & Koepke, J. (2015). Anatexis at the roof of an oceanic magma chamber at IODP Site 1256 (equatorial Pacific): An experimental study. *Contributions to Mineralogy and Petrology*, *169*(4), 39. https://doi.org/10.1007/s00410-015-1136-5

Erdmann, M., France, L., Fischer, L. A., Deloule, E., & Koepke, J. (2017). Trace elements in anatectic products at the roof of mid-ocean ridge magma chambers: An experimental study. *Chemical Geology*, *456*, 43–57. https://doi.org/10.1016/j.chemgeo.2017.03.004

Escartin, J., Smith, D. K., Cann, J., Schouten, H., Langmuir, C. H., & Escrig, S. (2008). Central role of detachment faults in accretion of slow-spreading oceanic lithosphere. *Nature*, *455*(7214), 790–794. https://doi.org/10.1038/nature07333

Fischer, L. A., Erdmann, M., France, L., Wolff, P. E., Deloule, E., Zhang, C., et al. (2016). Trace element evidence for anatexis at oceanic magma chamber roofs and the role of partial melts for contamination of fresh MORB. *Lithos*, *260*, 1–8. https://doi.org/10.1016/j.lithos.2016.05.001

France, L., Ildefonse, B., & Koepke, J. (2009). Interactions between magma and hydrothermal system in Oman ophiolite and in IODP Hole 1256D: Fossilization of a dynamic melt lens at fast spreading ridges. *Geochemistry, Geophysics, Geosystems*, *10*(10), Q10O19. https://doi.org/10.1029/2009gc002652

France, L., Koepke, J., Ildefonse, B., Cichy, S. B., & Deschamps, F. (2010). Hydrous partial melting in the sheeted dike complex at fast spreading ridges: Experimental and natural observations. *Contributions to Mineralogy and Petrology*, *160*(5), 683–704. https://doi.org/10.1007/s00410-010-0502-6

Garmany, J. (1989). Accumulations of melt at the base of young oceanic crust. *Nature*, *340*(6235), 628–632. https://doi.org/10.1038/340628a0

Goldstein, S. J., Perfit, M. R., Batiza, R., Fornari, D. J., & Murrell, M. T. (1994). Off-axis volcanism at the East Pacific Rise detected by uranium-series dating of basalts. *Nature*, *367*(6459), 157–159. https://doi.org/10.1038/367157a0

Grimes, C. B., Cheadle, M. J., John, B. E., Reiners, P. W., & Wooden, J. L. (2011). Cooling rates and the depth of detachment faulting at oceanic core complexes: Evidence from zircon Pb/U and (U-Th)/He ages. *Geochemistry, Geophysics, Geosystems*, *12*(3), Q0AG01. https://doi.org/10.1029/2010GC003391

Grimes, C. B., John, B., Cheadle, M., Mazdab, F., Wooden, J., Swapp, S., & Schwartz, J. (2009). On the occurrence, trace element geochemistry, and crystallization history of zircon from in situ ocean lithosphere. *Contributions to Mineralogy and Petrology*, *158*(6), 757–783. https://doi.org/10.1007/s00410-009-0409-2

Grimes, C. B., John, B. E., Cheadle, M., & Wooden, J. L. (2008). Protracted construction of gabbroic crust at a slow-spreading ridge: Constraints from $^{206}Pb/^{238}U$ zircon ages from Atlantis Massif and IODP Hole U1309D (30°N, MAR). *Geochemistry, Geophysics, Geosystems*, *9*(8), Q08012. https://doi.org/10.1029/2008GC002063

Hayman, N. W., Rioux, M., Anma, R., Tani, K., Dunkley, D. J., Crowley, J., & Schmitz, M. (2019). Accretion and oxidation of a superfast-spread axial melt lens: TIMS and SIMS zircon analyses of the IODP Hole 1256D gabbros. *Lithos*, *348*, 105184. https://doi.org/10.1016/j.lithos.2019.105184

Hiess, J., Condon, D. J., McLean, N., & Noble, S. R. (2012). 238U/235U systematics in terrestrial uranium-bearing minerals. *Science*, *335*(6076), 1610–1614. https://doi.org/10.1126/science.1215507

Hooft, E. E. E., Detrick, R. S., & Kent, G. M. (1997). Seismic structure and indicators of magma budget along the Southern East Pacific Rise. *Journal of Geophysical Research*, *102*(B12), 27319–27340. https://doi.org/10.1029/97jb02349

John, B. E., Foster, D. A., Murphy, J. M., Cheadle, M. J., Baines, A. G., Fanning, C. M., & Copeland, P. (2004). Determining the cooling history of in situ lower oceanic crust—Atlantis Bank, SW Indian Ridge. *Earth and Planetary Science Letters*, *222*(1), 145–160. https://doi.org/10.1016/j.epsl.2004.02.014

Karson, J. A., & Dick, H. J. B. (1983). Tectonics of ridge-transform intersections at the Kane Fracture Zone. *Marine Geophysical Researches*, *6*(1), 51–98. https://doi.org/10.1007/bf00300398

Koepke, J., Christie, D. M., Dziony, W., Holtz, F., Lattard, D., Maclennan, J., et al. (2008). Petrography of the dike-gabbro transition at IODP Site 1256 (equatorial Pacific): The evolution of the granoblastic dikes. *Geochemistry, Geophysics, Geosystems*, *9*(7), Q07O09. https://doi.org/10.1029/2008gc001939

Koepke, J., France, L., Müller, T., Faure, F., Goetze, N., Dziony, W., & Ildefonse, B. (2011). Gabbros from IODP Site 1256, equatorial Pacific: Insight into axial magma chamber processes at fast spreading ocean ridges. *Geochemistry, Geophysics, Geosystems*, *12*(9), Q09014. https://doi.org/10.1029/2011gc003655

Lagabrielle, Y., Bideau, D., Cannat, M., Karson, J. A., & Mével, C. (1998). Ultramafic-mafic plutonic rocks suites exposed along the Mid-Atlantic Ridge (10°N–30°N) Symmetrical-asymmetrical distribution and implications for seafloor spreading processes. In W. Buck, P. T. Delaney, J. A. Karson, & Y. Lagabrielle (Eds.), *Faulting and Magmatism at Mid-Ocean Ridges* (pp. 153–176). American Geophysical Union.

Lissenberg, C. J., Rioux, M., MacLeod, C. J., Bowring, S. A., & Shimizu, N. (2016). Crystallization depth beneath an oceanic detachment fault (ODP Hole 923A, Mid-Atlantic Ridge). *Geochemistry, Geophysics, Geosystems*, *17*(1), 162–180. https://doi.org/10.1002/2015gc006027

Lissenberg, C. J., Rioux, M., Shimizu, N., Bowring, S. A., & Mevel, C. (2009). Zircon dating of oceanic crustal accretion. *Science*, *323*(5917), 1048–1050. https://doi.org/10.1126/science.1167330

Lissenberg, J., Condon, D., Smye, A., & Anma, R. (2023). Zircon U-Pb data for plutonic rocks from IODP Hole 1256D, eastern equatorial Pacific Ocean [Dataset]. NERC EDS National Geoscience Data Centre. https://doi.org/10.5285/c7be6416-8814-46aa-b867-5dc2d1870e86

MacLeod, C. J., Escartin, J., Banerji, D., Banks, G. L., Gleeson, M., Irving, D. H. B., et al. (2002). Direct geological evidence for oceanic detachment faulting: The Mid-Atlantic Ridge, 15°45′N. *Geology*, *30*(10), 879–882. https://doi.org/10.1130/0091-7613(2002)030<0879:dgefod>2.0.co;2

Marjanović, M., Carbotte, S. M., Carton, H. D., Nedimović, M. R., Canales, J. P., & Mutter, J. C. (2018). Crustal magmatic System beneath the East Pacific Rise (8°20′ to 10°10′N): Implications for Tectonomagmatic Segmentation and crustal melt Transport at Fast-Spreading Ridges. *Geochemistry, Geophysics, Geosystems*, *19*(11), 4584–4611. https://doi.org/10.1029/2018gc007590

Martínez, F., Hey, R. N., & Johnson, P. D. (1997). The East ridge system 28.5–32°S East Pacific Rise: Implications for overlapping spreading center development. *Earth and Planetary Science Letters*, *151*(1–2), 13–31. https://doi.org/10.1016/s0012-821x(97)00095-2

McLean, N. M., Bowring, J. F., & Bowring, S. A. (2011). An algorithm for U-Pb isotope dilution data reduction and uncertainty propagation. *Geochemistry, Geophysics, Geosystems*, *12*(6), Q0AA18. https://doi.org/10.1029/2010gc003478

McLean, N. M., Condon, D. J., Schoene, B., & Bowring, S. A. (2015). Evaluating uncertainties in the calibration of isotopic reference materials and multi-element isotopic tracers (EARTHTIME Tracer Calibration Part II). *Geochimica et Cosmochimica Acta*, *164*, 481–501. https://doi.org/10.1016/j.gca.2015.02.040

Mével, C., Cannat, M., Gente, P., Marion, E., Auzende, J. M., & Karson, J. A. (1991). Emplacement of deep crustal and mantle rocks on the west wall of the MARK area (Mid-Atlantic Ridge, 23°N). *Tectonophysics*, *190*(1), 31–53. https://doi.org/10.1016/0040-1951(91)90353-t

Michael, P. J., Langmuir, C. H., Dick, H. J. B., Snow, J. E., Goldstein, S. L., Graham, D. W., et al. (2003). Magmatic and amagmatic seafloor spreading at the slowest mid-ocean ridge: Gakkel Ridge, Arctic Ocean. *Nature*, *423*(6943), 956–961. https://doi.org/10.1038/nature01704

Mutter, J. C., Carbotte, S. M., Su, W., Xu, L., Buhl, P., Detrick, R. S., et al. (1995). Seismic images of active magma systems beneath the East Pacific Rise between 17°05′ and 17°35′S. *Science*, *268*(5209), 391–395. https://doi.org/10.1126/science.268.5209.391

Neo, N., Yamazaki, S., & Miyashita, S. (2009). Data report: Bulk rock compositions of samples from the IODP Expedition 309/312 sample pool, ODP Hole 1256D. In D. A. H. Teagle, J. C. Alt, S. Umino, S. Miyashita, N. R. Banerjee, D. S. Wilson (Eds.),, & Expedition 309/312 Scientists (Eds.), *Proceedings of the Integrated Ocean Drilling Program*. Integrated Ocean Drilling Program Management International, Inc.

Phipps Morgan, J., & Chen, Y. (1993). Dependance of ridge-axis morphology on magma supply and spreading rate. *Nature*, *364*(6439), 706–708. https://doi.org/10.1038/364706a0

Purdy, G. M., Kong, L. S. L., Christeson, G. L., & Solomon, S. C. (1992). Relationship between spreading rate and the seismic structure of mid-ocean ridges. *Nature*, *355*(6363), 815–817. https://doi.org/10.1038/355815a0

Rioux, M., Bowring, S., Kelemen, P., Gordon, S., Dud·s, F., & Miller, R. (2012). Rapid crustal accretion and magma assimilation in the Oman-U.A.E. ophiolite: High precision U-Pb zircon geochronology of the gabbroic crust. *Journal of Geophysical Research*, *117*(B7), B07201. https://doi.org/10.1029/2012jb009273

Rioux, M., Cheadle, M. J., John, B. E., & Bowring, S. A. (2016). The temporal and spatial distribution of magmatism during lower crustal accretion at an ultraslow-spreading ridge: High-precision U–Pb zircon dating of ODP Holes 735B and 1105A, Atlantis Bank, Southwest Indian Ridge. *Earth and Planetary Science Letters*, *449*, 395–406. https://doi.org/10.1016/j.epsl.2016.05.047

Rioux, M., Jöns, N., Bowring, S., Lissenberg, C. J., Bach, W., Kylander-Clark, A., et al. (2015). U-Pb dating of interspersed gabbroic magmatism and hydrothermal metamorphism during lower crustal accretion, Vema lithospheric section, Mid-Atlantic Ridge. *Journal of Geophysical Research: Solid Earth*, *120*(4), 2093–2118. https://doi.org/10.1002/2014jb011668

Rioux, M., Lissenberg, C. J., McLean, N., Bowring, S. A., MacLeod, C. J., Hellebrand, E., & Shimizu, N. (2012). Protracted timescales of lower crustal growth at the fast-spreading East Pacific Rise. *Nature Geoscience*, *5*(4), 275–278. https://doi.org/10.1038/ngeo1378

Sano, T., Sakuyama, T., Ingle, S., Rodriguez, S., & Yamasaki, T. (2011). Petrological relationships among lavas, dikes, and gabbros from Integrated Ocean Drilling Program Hole 1256D: Insight into the magma plumbing system beneath the East Pacific Rise. *Geochemistry, Geophysics, Geosystems*, *12*(6), Q06013. https://doi.org/10.1029/2011gc003548

Schlindwein, V., & Schmid, F. (2016). Mid-ocean-ridge seismicity reveals extreme types of ocean lithosphere. *Nature*, *535*(7611), 276–279. https://doi.org/10.1038/nature18277

Schmitt, A. K., Perfit, M. R., Rubin, K. H., Stockli, D. F., Smith, M. C., Cotsonika, L. A., et al. (2011). Rapid cooling rates at an active mid-ocean ridge from zircon thermochronology. *Earth and Planetary Science Letters*, *302*(3–4), 349–358. https://doi.org/10.1016/j.epsl.2010.12.022

Schoolmeesters, N., Cheadle, M. J., John, B. E., Reiners, P. W., Gee, J., & Grimes, C. B. (2012). The cooling history and the depth of detachment faulting at the Atlantis Massif oceanic core complex. *Geochemistry, Geophysics, Geosystems*, *13*(10), Q0AG12. https://doi.org/10.1029/2012gc004314

Schwartz, J. J., John, B. E., Cheadle, M. J., Miranda, E. A., Grimes, C. B., Wooden, J. L., & Dick, H. J. B. (2005). Dating the growth of oceanic crust at a slow-spreading ridge. *Science*, *310*(5748), 654–657. https://doi.org/10.1126/science.1116349

Schwartz, J. J., John, B. E., Cheadle, M. J., Reiners, P. W., & Baines, A. G. (2009). Cooling history of Atlantis Bank oceanic core complex: Evidence for hydrothermal activity 2.6 Ma off axis. *Geochemistry, Geophysics, Geosystems*, *10*(8), Q08020. https://doi.org/10.1029/2009gc002466

Schwartz, J. J., John, B. E., Cheadle, M. J., Wooden, J. L., Mazdab, F., Swapp, S., & Grimes, C. B. (2010). Dissolution–reprecipitation of igneous zircon in mid-ocean ridge gabbro, Atlantis Bank, Southwest Indian Ridge. *Chemical Geology*, *274*(1–2), 68–81. https://doi.org/10.1016/j.chemgeo.2010.03.017

Sims, K. W. W., Blichert-Toft, J., Fornari, D. J., Perfit, M. R., Goldstein, S. J., Johnson, P., et al. (2003). Aberrant youth: Chemical and isotopic constraints on the origin of off-axis lavas from the East Pacific Rise, 9°–10°N. *Geochemistry, Geophysics, Geosystems*, *4*(10), 8621. https://doi.org/10.1029/2002gc000443

Sinton, J. M., & Detrick, R. S. (1992). Mid-Ocean Ridge magma chambers. *Journal of Geophysical Research*, *97*(B1), 197–216. https://doi.org/10.1029/91jb02508

Smith, D. K., Cann, J. R., & Escartin, J. (2006). Widespread active detachment faulting and core complex formation near 13°N on the Mid-Atlantic Ridge. *Nature*, *442*(7101), 440–443. https://doi.org/10.1038/nature04950

Tartarotti, P., Fontana, E., & Crispini, L. (2009). Deformation pattern in a massive ponded lava flow at ODP-IODP Site 1256: A core and log approach. *Geochemistry, Geophysics, Geosystems*, *10*(5), Q05O17. https://doi.org/10.1029/2008gc002346

Teagle, D. A. H., Alt, J. C., Umino, S., Miyashita, S., Banerjee, N. R., Wilson, D. S., & the Expedition 309/312 Scientists. (2006). *Proceedings of the Integrated Ocean Drilling Program*, 309/312. Integrated Ocean Drilling Program Management International, Inc. https://doi.org/10.2204/iodp.proc.309312.101.2006

Teagle, D. A. H., Ildefonse, B., Blum, P., & the Expedition 335 Scientists. (2012). *Proceedings of the Integrated Ocean Drilling Program*, 335. Integrated Ocean Drilling Program Management International, Inc. https://doi.org/10.2204/iodp.proc.335.101.2012

Tominaga, M., & Umino, S. (2010). Lava deposition history in ODP Hole 1256D: Insights from log-based volcanostratigraphy. *Geochemistry, Geophysics, Geosystems*, *11*(5), Q05003. https://doi.org/10.1029/2009gc002933

Umino, S., Crispini, L., Tartarotti, P., Teagle, D. A., Alt, J. C., Miyashita, S., & Banerjee, N. R. (2008). Origin of the sheeted dike complex at superfast spread East Pacific Rise revealed by deep ocean crust drilling at Ocean Drilling Program Hole 1256D. *Geochemistry, Geophysics, Geosystems*, *9*(6), Q06O08. https://doi.org/10.1029/2007gc001760

Veloso, E. E., Hayman, N. W., Anma, R., Tominaga, M., González, R. T., Yamazaki, T., & Astudillo, N. (2014). Magma flow directions in the sheeted dike complex at superfast spreading mid-ocean ridges: Insights from IODP Hole 1256D, Eastern Pacific. *Geochemistry, Geophysics, Geosystems*, *15*(4), 1283–1295. https://doi.org/10.1002/2013gc004957

Vera, E. E., Mutter, J. C., Buhl, P., Orcutt, J. A., Harding, A. J., Kappus, M. E., et al. (1990). The structure of 0 to 0.2 m.y. old oceanic crust at 9°N on the East Pacific Rise from expanded spread profiles. *Journal of Geophysical Research*, *95*(B10), 15529–15556. https://doi.org/10.1029/jb095ib10p15529

White, R. S., McKenzie, D., & O'Nions, R. K. (1992). Oceanic crustal thickness from seismic measurements and rare earth element inversions. *Journal of Geophysical Research*, *97*(B13), 19683–19715. https://doi.org/10.1029/92jb01749

Wilson, D., Hallenborg, E., Harding, A., & Kent, G. (2003). Data report: Site survey results from cruise EW9903. In D. Wilson, D. Teagle, G. Acton, et al. (Eds.), *Proceedings of the ODP, Initial Reports* (pp. 1–49). Ocean Drilling Program.

Wilson, D. S. (1996). Fastest known spreading on the Miocene Cocos-Pacific plate boundary. *Geophysical Research Letters*, *23*(21), 3003–3006. https://doi.org/10.1029/96gl02893

Wilson, D. S., Teagle, D. A. H., Acton, G. D., et al. (2003). *Proceedings of the ODP, Initial Reports*, 206. Ocean Drilling Program. https://doi.org/10.2973/odp.proc.ir.206.101.2003

Wilson, D. S., Teagle, D. A. H., Alt, J. C., Banerjee, N. R., Umino, S., Miyashita, S., et al. (2006). Drilling to gabbro in intact ocean crust. *Science*, *312*(5776), 1016–1020. https://doi.org/10.1126/science.1126090

Yamazaki, S., Neo, N., & Miyashita, S. (2009). Data report: Whole-rock major and trace elements and mineral compositions of the sheeted dike–gabbro transition in ODP Hole 1256D. In D. A. H. Teagle, J. C. Alt, S. Umino, S. Miyashita, N. R. Banerjee, D. S. Wilson, & the Expedition 309/312 Scientists, *Proceedings of the Integrated Ocean Drilling Program*, 309/312. Integrated Ocean Drilling Program Management International, Inc. https://doi.org/10.2204/iodp.proc.309312.203.2009

Zhang, C., Koepke, J., France, L., & Godard, M. (2017). Felsic Plutonic Rocks from IODP Hole 1256D, Eastern Pacific: Implications for the nature of the axial melt lens at fast-spreading mid-ocean ridges. *Journal of Petrology*, *58*(8), 1535–1565. https://doi.org/10.1093/petrology/egx064